Available online at www.sciencedirect.com

ScienceDirect

Procedia CIRP 133 (2025) 376–381

www.elsevier.com/locate/procedia

20th CIRP Conference on Modeling of Machining Operations

Simulation of chip formation for varying uncut chip thickness during vibration-assisted drilling with the CEL method

L. Schumski[a,b,*], F. Ducobu[c], L. Langenhorst[a,b], J. Sölter[a,b], B. Karpuschewski[a,b]

[a]Leibniz Institute for Materials Engineering IWT, Badgasteiner Straße 3, 28359 Bremen, Germany
[b]University of Bremen, MAPEX Center for Materials and Processes, Bibliothekstraße 1, 28359 Bremen, Germany
[c]University of Mons (UMONS), Faculty of Engineering (FPMs), Machine Design and Production Engineering Lab, 20 Place du Parc, B-7000 Mons, Belgium

* Corresponding author. Tel.: +49-421-218-51152; fax: +49-421-218-51102. *E-mail address:* schumski@iwt-bremen.de

Abstract

Vibration-assisted drilling is particularly efficient for long-chipping and difficult-to-machine materials due to its special kinematics with interrupted cutting. In order to optimize the process, a deeper understanding of the occurring external and internal material loads is required. For this purpose, a model is developed and simulation results are compared with experimental data on the materials Ti6Al4V and AISI 4140. Based on a kinematic simulation, individual segments on the main cutting edge are considered and the local chip formation is modelled as an orthogonal cut using the CEL method. Special consideration is given to the process kinematics, where, in addition to the entry and exit of the tool cutting edge, a varying uncut chip thickness occurs. Drilling without vibration assistance is also modelled in this way. The resulting drilling torques and thrust forces are compared with experimental data. The experiments are carried out on tubes with different internal diameters to represent the different segments of the main cutting edge. In addition, experimental results on drilling a rod and into solid material quantify the effects of the chisel edge and the minor cutting edges. The results show that both drilling and vibration-assisted drilling can be modelled using orthogonal cutting models with acceptable computation times.

Peer-review under responsibility of the scientific committee of the 20th CIRP Conference on Modeling of Machining Operations in Mons

Keywords: Drilling; Finite element method (FEM); Vibration-assisted drilling

1. Introduction

Low frequency vibration-assisted drilling represents a promising alternative to conventional drilling when it comes to difficult-to-machine and long-chipping materials [1, 2]. By adjusting its frequency and amplitude chip breaking and interrupted cutting can be enforced, typically within one tool rotation [3-5]. This has the potential to solve several difficulties in drilling, e.g. an increasing workpiece temperature with increasing drilling depth [6] and poor chip removal affecting the quality of the bore hole [1] and its surface integrity [2]. Compared to drilling, the workpiece temperatures are approx. 43 % lower [5]. On the other hand, vibration-assisted drilling normally results in higher mechanical peak loads [7-9]. By further adapting the process kinematics, Paulsen et al. and Schumski et al. were able to lower mechanical loads [8, 9].

Machining parameters for vibration-assisted drilling are, for now, mostly determined based on experience. Brinksmeier et al. published a straightforward kinematic model for the movement of both cutting edges of a drill when an axial vibration amplitude is superimposed on the linear feed [4]. Similar approaches supporting the process design can be found in [3]. For drilling without vibration assistance, several studies have focused on predicting mechanical and thermal loads by means of numerical chip formation simulations [10-12]. In addition to different materials and machining parameters,

2212-8271
Peer-review under responsibility of the scientific committee of the 20th CIRP Conference on Modeling of Machining Operations in Mons
10.1016/j.procir.2025.02.065

different formulation methods were used. In addition to the Lagrangian formulation, the Coupled Eulerian-Lagrangian (CEL) method has become increasingly popular in recent years [13-15], e.g. Ducobu et al. obtained results with high accuracy using a quasi-2D orthogonal simulation [16]. 3D models for drilling using the CEL method also delivered promising results [10, 11, 17]. However, a varying uncut chip thickness as it occurs in vibration-assisted drilling is not part of these investigations. Schulze et al. found no significant deviations between modeling broaching with varying uncut chip thickness by vertical tool movement or adjustment of the workpiece shape [18]. Avevor et al. were able to model varying uncut chip thickness by using an Arbitrary Lagrangian Eulerian (ALE) model [19]. In previous studies on 3D chip formation models of vibration-assisted drilling, Schumski et al. found that finite element length is crucial for the prediction quality and, until now, no satisfying results have been calculated, even with element lengths down to 10 µm and associated high computational demands [9, 17]. Since in vibration-assisted drilling the axial vibration amplitude of the tool is specifically selected to ensure interrupted cutting with an entry and exit of the cutting edge, an even finer mesh seems to be necessary in these phases. Given the even higher computation times resulting from this, in this work, a more efficient (quasi) 2D numerical chip formation model was developed and utilized.

2. Objective and Procedure

In order to optimize low frequency vibration-assisted drilling in terms of beneficial process parameters and cutting edge geometry in the future, the objective of this work is the prediction and analysis of drilling torque and thrust force when uncut chip thickness varies over time. For this purpose, a modeling approach was developed, presented within the overall procedure in Fig. 1. Based on fixed process parameters derived from previous experimental studies [8], a kinematic model (cf. section 3.1) calculates the local uncut chip thickness $h(t)$ and local cutting velocity v_c for different positions along the main cutting edge of the tool. Both quantities, together with measured local cutting edge radius r_β, local clearance angle α, and local rake angle γ, were used as input for the numerical chip formation model (cf. section 3.2). In this model, orthogonal cutting conditions are assumed and the resulting specific cutting force $F_c'(t)$ and normal force $F_{cN}'(t)$ were calculated. By integrating these specific forces along the cutting edge, the drilling torque $M_{z,sim}(t)$ and the thrust force $F_{z,sim}(t)$ can be determined and compared to measurements (cf. section 4).

The orthogonal cutting conditions assumed in the modeling approach are not valid for the chisel edge and its transition area to the main cutting edge. Therefore, in this first attempt, only the main cutting edges are examined by using tubes with different inner bore hole diameters as workpieces. In addition to tube A and tube B, where these conditions are met and only the main cutting edges are in contact, a rod, and a solid geometry are investigated in the experiments (Table 1). This allows a determination of the proportion each cutting edge area contributes to the total process loads. To initially verify the modeling approach, simulations and experiments are also conducted for the simpler drilling kinematics without vibration. The same workpiece geometries and process parameters were used, but the feed was doubled to achieve a similar load level. For both process kinematics, simulations and experiments were conducted for titanium alloy Ti6Al4V and steel AISI 4140 in a ferritic-pearlitic state.

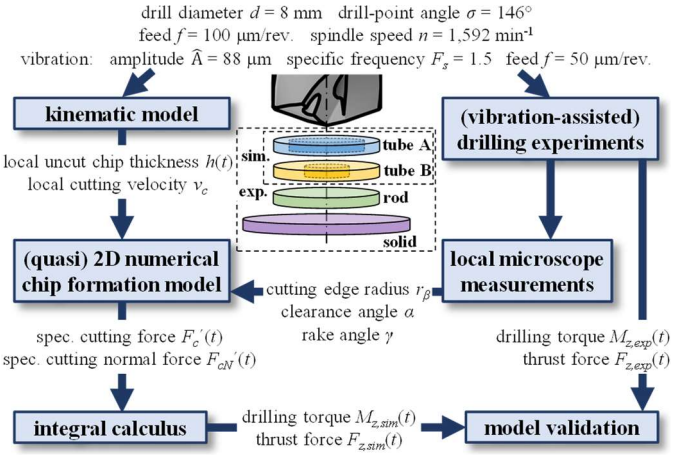

Fig. 1. Overall procedure and modeling approach for the prediction of drilling torque and thrust force in (vibration-assisted) drilling of different workpieces.

Table 1. Details on investigated workpiece geometries.

workpiece label	tube A	tube B	rod	solid
outer diameter d_1 (mm)	7.6	7.6	7.6	12
inner diameter d_2 (mm)	5.4	3.2	-	-

3. Modeling approach

3.1. Kinematic model

For vibration-assisted drilling, the position in feed direction of the two cutting edges $z_{f1/2}$ in dependence of rotation angle φ can be calculated by equation 1. Considering the phase-shift between the first cutting edge ($\varphi_{0,1}$ = 0°) and the second cutting edge ($\varphi_{0,2}$ = 180°) as well as the process parameters in Fig. 1, a stationary shape of the borehole bottom topography is generated after four tool revolutions. With further movement of the cutting edges, interrupted cutting results, and for both cutting edges the penetration in feed direction $f_{vib}(t)$ varies between zero and a calculated maximum, which is smaller than the sum of feed per tooth f_z and vibration amplitude $\hat{A}$.

$$z_{f1/2} = -f \cdot \varphi / 360° + \hat{A} \cdot \sin(F_s \cdot \varphi + \varphi_{0,1/2}) \quad (1)$$

The uncut chip thickness can be calculated by considering the drill-point angle σ according to $h(t) = f_{vib}(t) \cdot \sin(\sigma/2)$. The resulting profile of the uncut chip thickness $h(t)$ is trapezoidal according to equation 2 and repeats with frequency of $F_s \cdot n$ = 39.8 Hz simultaneously for both cutting edges independent of the position along the cutting edge.

$$h = \begin{cases} 28.5\ \mu m/ms \cdot t & , \ 0\ ms \le t < 3.4\ ms \\ 95.6\ \mu m & , \ 3.4\ ms \le t < 6.3\ ms \\ -28.5\ \mu m/ms \cdot t + 274.8\ \mu m & , \ 6.3\ ms \le t < 9.7\ ms \\ 0\ \mu m & , \ 9.7\ ms \le t < 25.1\ ms \end{cases} \quad (2)$$

3.2. Numerical chip formation model

Chip formation in orthogonal cutting was simulated by (quasi) 2D finite element models. They were developed with Abaqus/Explicit 2022 (double precision) and the CEL formulation was adopted. This formulation is only available in 3D but adequate boundary conditions were applied to satisfy plane strain conditions with one element in the out-of-plane direction with element length of 50 µm [16, 20]. The workpiece is modelled as a Eulerian body with element type EC3D8RT to avoid mesh deformation, while the tool is a Lagrangian body with element type C3D8T. This implies it is mandatory to mesh the area above the workpiece to capture the chip formation as shown in Fig. 2 (Initial void). In order to reduce computation time, the size of the mesh representing the workpiece was adjusted and a mass scaling factor of 1000 was implemented. Element size in the area close to the cutting edge radius of the tool and in the upper layer of the workpiece is 5 µm × 5 µm based on the results of a previous mesh sensitivity study carried out for the same value of cutting edge radius [16].

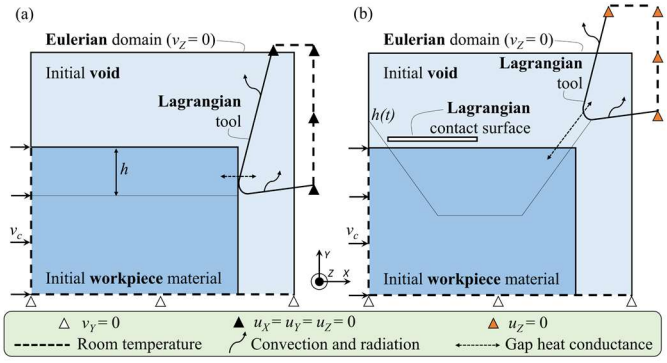

Fig. 2. Configuration of (a) drilling and (b) vibration-assisted drilling.

Workpiece materials have an elasto-plastic behavior with an inelastic heat fraction of 0.9. The materials behavior is described by Johnson-Cook approach in equation 3 [21].

$$\sigma_y = (A + B \cdot \varepsilon^n) \cdot \left(1 + C \cdot \ln \frac{\dot{\varepsilon}}{\dot{\varepsilon}_0}\right) \cdot \left(1 - \left[\frac{T - T_{room}}{T_{melt} - T_{room}}\right]^m\right) \quad (3)$$

The tool is made of tungsten carbide and has a linear elastic behavior. Friction is modelled using Coulomb's assumption. The efficiency of the conversion of friction energy into heat energy is 100 % and the generated heat energy is equally distributed between the tool and the workpiece.

For Ti6Al4V, the parameters of the Johnson-Cook model and the value of Coulomb's friction coefficient were retrieved from an AI-based inverse identification [22]. For AISI 4140 steel in a ferritic-pearlitic state, Johnson-Cook parameters, determined by means of a microstructure-based material model [23], and friction coefficient were taken from [24]. In the friction model, a shear stress limit, estimated by the initial yield stress, was implemented. Johnson-Cook and friction parameters are provided in Table 2 for both materials.

Radiation with an emissivity of $\epsilon = 0.3$ [25] and convection with $U = 50$ W/m²K [26] are included only for the Lagrangian body as they are not available for the Eulerian one. Pressure-based gap conductance at the tool-workpiece interface is included [27]. Material properties are provided in Table 3.

Table 2. Johnson-Cook and Coulomb model parameters [22, 24].

parameter	Ti6Al4V	AISI 4140
A (MPa)	997.9	510
B (MPa)	331.2	480
n	0.54	0.25
m	0.714	1.46
C	0.0313	0.018
$\dot{\varepsilon}_0$	1	0.002
T_{melt} (K)	1878	1809
μ	0.28	0.7
τ_{max} (MPa)	-	$A / \sqrt{3} = 295$

Table 3. Materials properties [28-31].

material property	Ti6Al4V	AISI 4140	WC
Young's modulus, E (GPa)	113.8	205.126	800
Poisson's ratio, υ	0.34	0.3	0.2
density, ρ (kg/m³)	4430	7612	15,000
conductivity, k (W/mK)	7.3	40.38	100
expansion, α (K^{-1})	$8.6 \cdot 10^{-6}$	$10.79 \cdot 10^{-6}$	$5 \cdot 10^{-6}$
specific heat, c_p (J/kgK)	580	447.04	202

Two different simulations were developed: with and without vibration assistance. For the modeling without vibration assistance, six tool geometry-cutting conditions couples were considered to approximate drilling with the orthogonal cutting assumption. Local cutting speeds were calculated along the main cutting edge of the drill acc. to their radial distance r and tool geometry was measured by optical measuring device InfiniteFocus G5, Bruker Alicona, cf. Table 4. As the actual tool movement during experiments is only considered in the kinematic model to calculate the uncut chip thickness, the measured clearance and rake angles were used instead of effective angles. The uncut chip thickness was constant with $h = f_z \cdot \sin(\sigma/2) = 48$ µm. This results in six models with the same uncut chip thickness, but with a different tool geometry-cutting speed couple. The boundary conditions are a fixed tool and a workpiece moving horizontally at the cutting speed as shown in Fig. 2 (a).

Table 4. Cutting speed and tool geometry depending on the position along the main cutting edge according to the radial distance.

radial distance, r (mm)	1.6	2.0	2.4	2.8	3.2	3.6
cutting speed, v_c (m/min)	16	20	24	28	32	36
rake angle, γ_0 (°)	10	15	18	21	24	26.5
clearance angle, α_0 (°)	10					
cutting edge radius, r_β (µm)	20					

For the modelling with vibration assistance, the same six positions along the main cutting edge of the drill were considered with the same cutting speed and tool geometry. Vibration was introduced according to the kinematic model and equation 2 for the uncut chip thickness. The boundary conditions were updated to include them as shown in Fig. 2 (b): the tool now moves vertically to allow the change in the uncut chip thickness value, while the workpiece still moves

horizontally at the cutting speed. Chip curl can result in contact with the upper workpiece surface. To avoid non-physical merging of the Eulerian chip with the Eulerian workpiece, a Lagrangian frictionless contact surface with the same material as the workpiece has been adopted.

4. Experimental setup

Experiments on vibration-assisted drilling were conducted on a modified machining center DMU 80E, Deckel Maho (Fig. 3). The magnetic bearing spindle of type LeviSpin, Keba, was used with a solid carbide twist drill with TiAlN coating of type WTX-TI.8,00.R.5D.IK.HA DPA54, Ceratizit. In order to meet the boundary conditions of the numerical model, no cooling lubricant was used. In accordance with Fig. 1 and Table 1 different workpiece geometries were prepared by sawing, turning, and pre-drilling of bars. Workpiece materials used were Ti6Al4V in Grade 5 acc. to ASTM standard and AISI 4140 heat treated to a ferritic-pearlitic state (heating 10 K/min / 850 °C for 120 min / cooling in furnace 1.7 K/min). During cutting, the drilling torque and forces were measured by a dynamometer of type 9272, Kistler, with a 1 kHz low-pass filter and a 2.5 kHz sampling rate. The tool was replaced after drilling four workpiece geometries two times (one repetition). The experiments for drilling without vibration assistance were carried out on a machining centre DMC 65V, Deckel Maho.

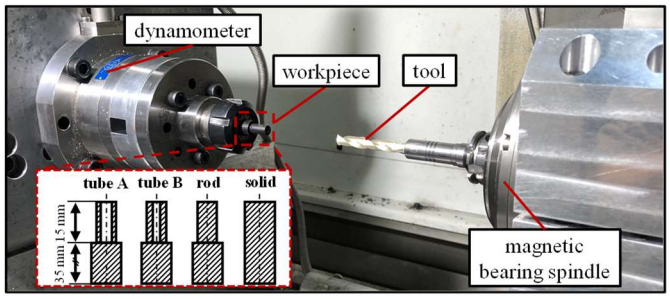

Fig. 3. Experimental setup for vibration-assisted drilling.

The data for drilling without vibration assistance was analysed by mean value and standard deviation for the steady state. In case of vibration-assisted drilling, a python script was used to evaluate each tool engagement signal regarding its maximum drilling torque and thrust force as well as its engagement time. For comparison with simulations, signals representing the mean of these values were selected.

5. Results and Discussion

5.1. Numerical simulation results on orthogonal cutting

The (quasi) 2D numerical chip formation model was used to calculate specific forces for different cutting speeds and rake angles acc. to the radial distances in Table 4. For the radial distance $r = 2.8$ mm, Fig. 4 shows the evolution of the specific forces over time for constant uncut chip thickness (drilling) and varying uncut chip thickness (vibration-assisted drilling) and for both workpiece materials. In the first case, a steady state is reached within the first millisecond, indicating a 7 % higher specific cutting force but a 42 % lower specific cutting normal force for AISI 4140 than for Ti6AlV. The same order is true for the second case (vibration-assisted drilling). Here, the specific cutting forces follow the varying uncut chip thickness acc. to equation 2. Regarding the specific cutting normal forces, a constant level during constant uncut chip thickness can be found, too. However, increasing uncut chip thickness results in decreasing cutting normal forces and vice versa, which is not known, e.g. from milling, and needs further investigations. This is true for both materials but more pronounced for AISI 4140 and for higher radial distances r (higher cutting speed and rake angle). Interestingly, this results in specific cutting normal forces during constant uncut chip thickness (green dotted curve) being sometimes even lower than the ones in the first case (orange dotted curve) although their uncut chip thickness is half of it.

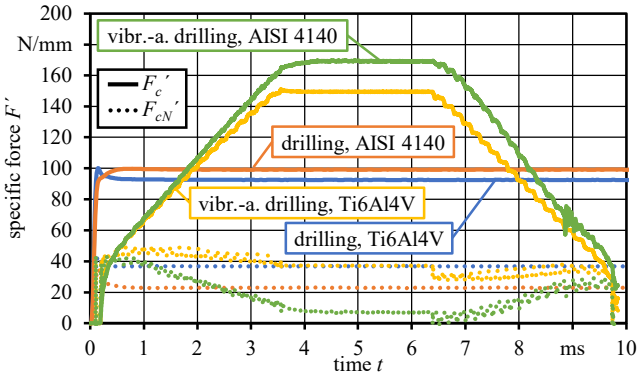

Fig. 4. Numerical simulation results on orthogonal cutting for $r = 2.8$ mm.

Fig. 5 shows the specific forces in dependence of the radial distance in case of drilling. Both force components decrease with higher cutting speed and rake angle due to thermal softening. The specific cutting normal force for Ti6Al4V is almost constant over the investigated range. The temporal resolved forces in case of vibration-assisted drilling show a similar behavior.

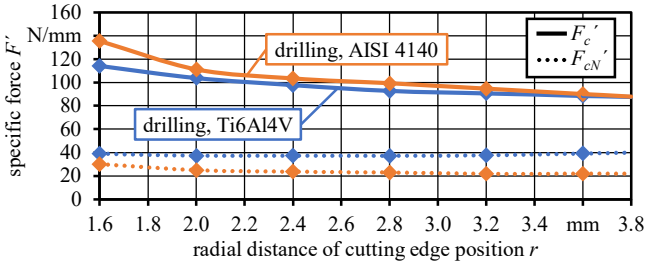

Fig. 5. Simulated specific forces along the main cutting edge in drilling.

5.2. Model validation for drilling without vibration assistance

Specific cutting forces $F_c'(r)$ and specific cutting normal forces $F_{cN}'(r)$ were used to calculate drilling torque and thrust force for both cutting edges in total by trapezoidal numerical integration over the variable running along the cutting edge $s = r / \sin(\sigma/2)$ according to equations 4 – 5. As drilling is usually described as oblique machining, the inclination angle should be taken into account when calculating the drilling torque and thrust force. Due to the minor influence of the inclination angle (< 0.1% acc. to [32]), this is neglected in the work.

$$M_z = \frac{2}{\sin(\sigma/2)} \cdot \int_{r_{start}}^{r_{end}} r \cdot F_c'(r)\, \mathrm{d}r \quad (4)$$

$$F_z = \frac{2}{\sin(\sigma/2)} \cdot \int_{r_{start}}^{r_{end}} \cos(90° - \sigma/2) \cdot F_{cN}'(r)\, \mathrm{d}r \quad (5)$$

Fig. 6 shows the calculated results for Ti6Al4V in comparison to measured drilling torques and thrust forces for the investigated workpiece geometries. The calculated drilling torques are in good agreement with measurements (tube A: -14 %, tube B: -13 %) and lie within their standard deviations for both simulated tubes. The thrust forces, however, are underestimated by the model (tube A: -55 %, tube B: -54 %), which is known from various other works and is associated with a neglection of an additional contact area at the flank face, e.g. due to tool wear, in chip formation models.

A comparison of the different workpiece geometries confirms the expectation of higher drilling torques and thrust forces when more material volume is cut. In terms of torque, the pre-drilled hole with diameter of 3.2 mm in tube B only leads to a decrease of -11 % compared to the rod, whereas the thrust force decreases by -44 %. This clearly outlines the effect of the drill's chisel edge, which is in contact only for the rod geometry. In comparison to the rod, drilling into solid material increases the drilling torque by 49 % and the thrust force by 14 %. Part of this increase is due to additional cut material volume. Moreover, friction between the minor cutting edges as well as chips and the bore hole wall has to be considered.

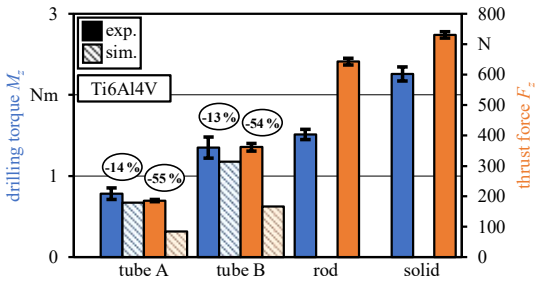

Fig. 6. Comparison of measured and calculated results for drilling Ti6Al4V without vibration assistance.

Almost the same deviations between simulations and measurements occur for drilling AISI 4140 (Fig. 7), i.e. drilling torque -11 % (tube A) and -13 % (tube B) and thrust force -50 % (tube A) and -55 % (tube B). As already discussed for the simulation results, drilling torques are higher and thrust forces are lower compared to Ti6Al4V. The effect of an inactive chisel edge between tube B and rod is - 26% in terms of drilling torque and -59 % in terms of thrust force and thus is more pronounced for AISI 4140. Drilling into solid material increases the drilling torque by 29 % and thrust force by 14 %.

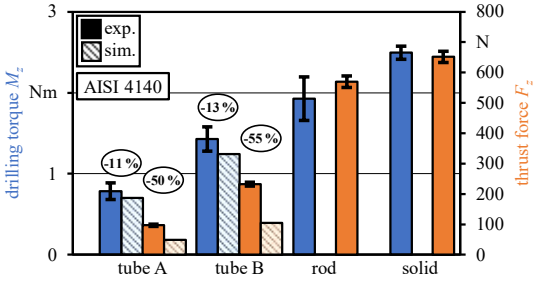

Fig. 7. Comparison of measured and calculated results for drilling AISI 4140 without vibration assistance.

5.3. Model validation for vibration-assisted drilling

Numerical integration was also conducted on the temporal resolved specific forces when the uncut chip thickness varies acc. to vibration-assisted drilling. Fig. 8 shows the comparison of simulation results with one statistically representative tool engagement from experiments for all investigated workpiece geometries. Qualitatively, findings from drilling without vibration assistance can be confirmed. The simulation is capable of predicting the drilling torque with high accuracy, although the measured signals for tube A and tube B show high-frequency oscillations due to the missing process stabilizing effect of an active chisel edge. Inaccuracies mainly occur in the entry and exit phases of the tool cutting edges, and more pronounced for Ti6Al4V, where the simulations show a steeper slope of drilling torque and thrust force and thus shorter time of engagement. A reason might be the neglection of the system compliance in the kinematic model. This might also be the reason that no constant level can be identified in the measurements when the uncut chip thickness, at least the one based on the kinematic model, is constant.

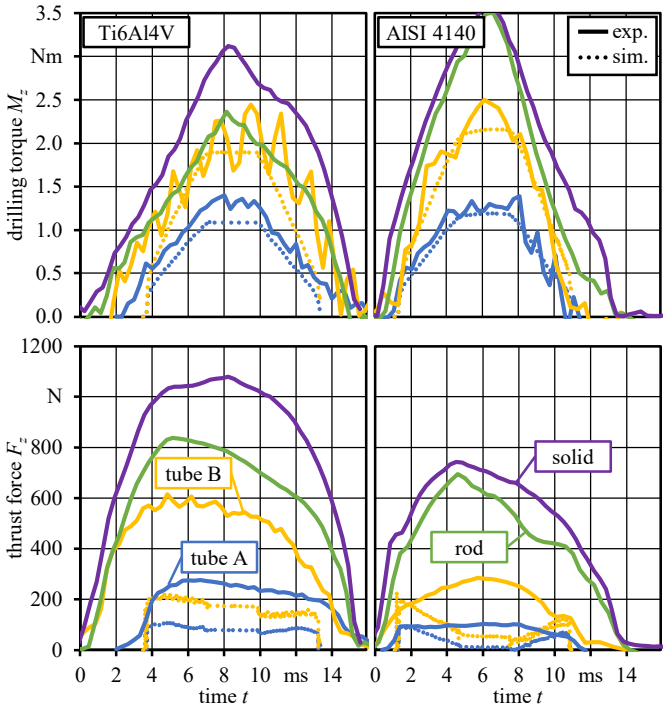

Fig. 8. Measured and calculated results for vibration-assisted drilling.

6. Summary and Outlook

The developed modeling approach on low frequency vibration-assisted drilling is able to calculate drilling torques in agreement to experiments by utilizing (quasi) 2D chip formation simulations under orthogonal cutting conditions with varying uncut chip thickness. It could be shown that calculated drilling torques for the two investigated materials Ti6Al4V and AISI 4140 lie within the standard deviation of measurements when drilling tubes with and without vibration assistance. This allows for a first attempt to optimize the process in terms of beneficial process parameters and cutting edge geometry in the future. As a major advantage compared to 3D chip formation

simulations shorter computation times can be reached and will reduce optimization effort.

For vibration-assisted drilling, deviations between measured and calculated drilling torques still occur at the entry and exit of the tool cutting edges. The neglection of elastic effects when calculating the uncut chip thickness in the presented approach might be the reason. This will be addressed in the future by considering a preformed workpiece in the chip formation simulation acc. to the revealed stationary shape of the borehole bottom topography after four tool revolutions.

Results also show underestimated cutting normal forces and thus thrust forces for drilling with and without vibration which needs further investigations, e.g. implementation of tool wear. The experimental results on drilling a rod and into solid material also confirm higher thrust forces, and also drilling torques, due to active chisel edge and minor cutting edges, which has to be considered in the future.

Acknowledgements

The research work was funded by the Deutsche Forschungsgemeinschaft (DFG, German Research Foundation) – 439950037.

References

[1] Biermann D, Iovkov I, Blum H, Rademacher A, Taebi K, Suttmeier FT, Klein N. Thermal Aspects in Deep Hole Drilling of Aluminium Cast Alloy Using Twist Drills and MQL. Procedia CIRP 2012;3:245-250.

[2] Kwong J, Axinte DA, Withers PJ. The sensitivity of Ni-based superalloy to hole making operations: Influence of process parameters on subsurface damage and residual stress. J Mater Procces Technol 2009;209(8):3968-3977.

[3] Deyuan Z, Lijiang W. Investigation of chip in vibration drilling. Int J Mach Tools Manuf 1998;38(3):165-176.

[4] Brinksmeier E, Pecat O, Rentsch R. Quantitative analysis of chip extraction in drilling of Ti6Al4V. CIRP Annals 2015;64(1):93-96.

[5] Pecat O, Brinksmeier E. Low Damage Drilling of CFRP/Titanium Compound Materials for Fastening. Procedia CIRP 2014;13:1-7.

[6] Bono M. Experimental and Analytical Issues in Drilling. Michigan: The University of Michigan; 1979.

[7] Paulsen T, Pecat O, Wagner A, Brinksmeier E. Modification of oscillation modes in low frequency vibration assisted drilling. Procedia Manuf 2017;14:1-7.

[8] Paulsen T, Guba N, Sölter J, Karpuschewski B. Influence of the workpiece material on the cutting performance in low frequency vibration assisted drilling. CIRP J Manuf Sci Technol 2020;31:140-152.

[9] Schumski L, Paulsen T, Sölter J, Karpuschewski B. Finite element simulation of low frequency vibration-assisted drilling with modification of oscillation modes. Procedia CIRP 2021;102:168-173.

[10] Priest J, Ghadbeigi H, Avar-Soberanis S, Gerardis S. 3D finite element modelling of drilling: The effect of modelling method. CIRP J Manuf Sci Technol 2021;35:158-168.

[11] Abdelhafeez AM, Soo SL, Aspinwall D, Dowson A, Arnold D, A Coupled Eulerian Lagrangian Finite Element Model of Drilling Titanium and Aluminium Alloys. SAE Int J Aerospace 2016;9(1):198-207.

[12] Wolf T, Fast M, Saelzer J, Brock G, Biermann D, Turek S. Modeling and validation of a FEM chip formation simulation to expand the numerical work on discontinuous drilling of Inconel 718. Procedia CIRP 2023;117:32-37.

[13] Ducobu F, Arrazola PJ, Rivière-Lorphèvre E, Zarate G, Madariaga A, Filippi E. The CEL Method as an Alternative to the Current Modelling Approaches for Ti6Al4V Orthogonal Cutting Simulation. Procedia CIRP 2017;58:245-250.

[14] Vovk A, Sölter J, Karpuschewski B. Finite element simulations of the material loads and residual stresses in milling utilizing the CEL method. Procedia CIRP 2020;87:539-544.

[15] Svensson D, Andersson T, Andersson Lassila A, Coupled Eulerian–Lagrangian simulation and experimental investigation of indexable drilling. The Int J Adv Manuf Technol 2022;121(1-2):471-486.

[16] Ducobu F, Rivière-Lorphèvre E, Filippi E. Mesh influence in orthogonal cutting modelling with the Coupled Eulerian-Lagrangian (CEL) method. European J Mech – A/Solids 2017;65:324-335.

[17] Schumski L, Tonn T, Buss L, Sölter J, Fritsching U, Karpuschewski B. Finite element simulation of the mechanical loads during low frequency vibration-assisted drilling utilizing the CEL-method. Procedia CIRP 2024;126:378-383.

[18] Schulze V, Boev N, Zanger F. Simulation of Metal Cutting Process with Variable Cutting Thickness During Broaching. Procedia CIRP 2012;1:437-442.

[19] Avevor Y, Vincent J, Faure L, Moufki A, Philippon S. An ALE approach for the chip formation process in high speed machining with transient cutting conditions: Modeling and experimental validation. Int J Mech Sci 2017;130:546-557.

[20] da Silva FAV, Outeiro JC. Machining simulation of Inconel 718 using Lagrangian and Coupled Eulerian-Lagrangian approaches. Procedia CIRP 2021;102453-458.

[21] Johnson G, Cook W. A constitutive model and data for metals subjected to large strains, high strain rates and high temperatures. Proc. 7th Int Symp Ballistics 1983;21: 541-547.

[22] Ducobu F, Kugalur-Palanisamy N, Briffoteaux G, Gobert M, Tuyttens D, Arrazola PJ Rivière-Lorphèvre E. Identification of the Constitutive and Friction Models Parameters via a Multi-Objective Surrogate-Assisted Algorithm for the Modeling of Machining - Application to Arbitrary Lagrangian Eulerian Orthogonal Cutting of Ti6Al4V. J Manuf Sci Eng 2024;146(6): 061005.

[23] Abouridouane M, Klocke F, Döbbeler B. Analytical temperature prediction for cutting steel. CIRP Annals 2016;65(1):77-80.

[24] Beblein S, Breidenstein B, Denkena B, Pusch C, Hoche H, Oechsner M. Thermomechanical Coating Load in Dependence of Fundamental Coating Properties. Procedia CIRP 2017;58:25-30.

[25] viZaar industrial imaging AG. Emissionsgrad-Tabelle. https://vizaar-xtra.de/emissionsgrad-tabelle/.01.11.2024.

[26] Schweizer A. https://www.schweizer-fn.de/stoff/wuebergang_gase/wuebergang_gase.php. 01.11.2024.

[27] Ducobu F, Palanisamy NK, Arrazola PJ, Rivière-Lorphèvre E. Application of material constitutive and friction models parameters identified with AI and ALE to a CEL orthogonal cutting model. Procedia CIRP 2023;117:311-316.

[28] Boivineau M, Cagran C, Doytier D, Eyraud V, Nadal MH, Wilthan B, Pottlacher G. Thermophysical Properties of Solid and Liquid Ti-6Al-4V (TA6V) Alloy. Int J Thermophys 2006;27(2):507-529.

[29] Spittel M, Spittel T, Warlimont H, Landolt H, Börnstein R, Martienssen W. Numerical data and functional relationships in science and technology. Landolt-Börnstein Group VIII Advanced Materials and Technologies. Berlin: Springer, 2011.

[30] Buchkremer S. Irreversible thermodynamics of nano-structural surface modifications in metal cutting. Aachen: Apprimus, 2017.

[31] GRANTA EduPack 2020. Granta Design Limited.

[32] Armarego EJA, Wright JD. Predictive models for drilling thrust and torque—a comparison of three flank configurations. CIRP Annals 1984; 33:5–10.